Author(s): Konu, Jari; Tuononen, Heikki; Chivers, Tristram

Title: Synthesis, X-ray structures and redox behaviour of the group 14 bis-boraamidinates M[PhB(μ-N-t-Bu)2]2 (M = Ge, Sn) and Li2M[PhB(μ-N-t-Bu)2]2 (M = Sn, Pb)

Year: 2009

Version:

Please cite the original version:

Konu, J., Tuononen, H., & Chivers, T. (2009). Synthesis, X-ray structures and redox behaviour of the group 14 bis-boraamidinates M[PhB(μ-N-t-Bu)2]2 (M = Ge, Sn) and Li2M[PhB(μ-N-t-Bu)2]2 (M = Sn, Pb). Canadian Journal of Chemistry, 87(3), 461-471. https://doi.org/10.1139/v08-183

Syntheses, X-ray structures and redox behaviour of the group 14 bis-boraamidinates M[PhB(μ-N-*t*-Bu)$_2$]$_2$ (M = Ge, Sn) and Li$_2$M[PhB(μ-N-*t*-Bu)$_2$]$_2$ (M = Ge, Sn, Pb)

Jari Konu, Heikki M. Tuononen, and Tristram Chivers

Jari Konu,[1] Heikki M. Tuononen[2] and Tristram Chivers[1, 3]

[1] Department of Chemistry, University of Calgary, Calgary, Alberta T2N 1N4, Canada

[2] Department of Chemistry, University of Jyväskylä, P.O. Box 35, Jyväskylä, FI-40014, Finland

[3] Corresponding author (e-mail: chivers@ucalgary.ca)

Abstract: The solid-state structures of the complexes M[PhB(μ-N-*t*-Bu)$_2$]$_2$ (**1a,** M= Ge; **1b**, M = Sn) were determined to be spirocyclic with two orthogonal boraamidinate (*bam*) ligands *N,N'*-chelated to the group 14 centre. Oxidation of **1b** with SO_2Cl_2 afforded the thermally unstable, blue radical cation {Sn[PhB(μ-N-*t*-Bu)$_2$]$_2$}$^{\bullet+}$, identified by EPR spectroscopy supported by DFT calculations, whereas the germanium analogue **1a** was inert towards SO_2Cl_2. The reaction between Li$_2$[PhB(μ-N-*t*-Bu)$_2$]$_2$ and $SnCl_2$ or PbI_2 in 2:1 molar ratio in diethyl ether produced the novel heterotrimetallic complexes Li$_2$Sn[PhB(μ-N-*t*-Bu)$_2$]$_2$ (**2b**) and (Et$_2$O·Li)LiPb[PhB(μ-N-*t*-Bu)$_2$]$_2$ (**2c**·OEt$_2$), respectively. By contrast, treatment of Li$_2$[PhB(μ-N-*t*-Bu)$_2$]$_2$ with $C_4H_8O_2$·$GeCl_2$ yielded the germanium(IV) complex **1a** via a redox process. The X-ray structures of **2b** and **2c**·THF revealed polycyclic arrangements in which one *bam* ligand is *N*,*N*′-chelated to the Sn(II) or Pb(II) atom and one of the Li^+ cations, while the second *bam* ligand exhibits a unique bonding mode, bridging all three metal centres. The fluctional behaviour of **2b** was investigated by variable temperature, multinuclear NMR spectroscopy

Introduction

The dianionic boraamidinate (*bam*) ligand, $[RB(NR')_2]^{2-}$ (**B**), is formally isoelectronic with the extensively studied monoanionic amidinate (*am*) ligand $[RC(NR')_2]^-$, (**A**). A wide range of main-group element and transition-metal complexes have been structurally characterized and a variety of bonding modes have been established for the *bam* ligand (1-3).

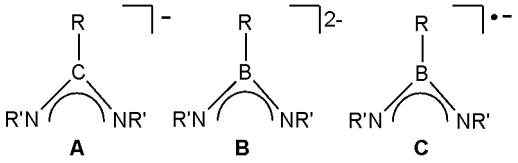

The most intriguing consequence of the 2- charge is the facile tendency for redox transformations to occur in which the dianion **B** is oxidized to the corresponding monoanion radical $[bam]^{\bullet-}$ (**C**). This paramagnetic ligand can be stabilized through chelation, e.g., to early main-group metals (4, 5). In the case of group 13 metals it has been possible to isolate *stable* neutral radicals. For example, the intensely coloured paramagnetic species $\{M[PhB(\mu\text{-}N\text{-}t\text{-}Bu)_2]_2\}^{\bullet}$ (M = Al, dark red; M = Ga, Dark green) are produced by one-electron oxidation of the corresponding anions with iodine, and the X-ray structures of these spirocyclic complexes have been determined (Scheme 1) (4). The SOMO of these neutral radicals is located primarily and equally in p-orbitals on the four nitrogen atoms of the two *bam* ligands; there is very little electron density on the group 13 centres.

Scheme 1. Synthesis of spirocyclic $\{M[PhB(\mu\text{-}N\text{-}t\text{-}Bu)_2]_2\}^{\bullet}$ radicals

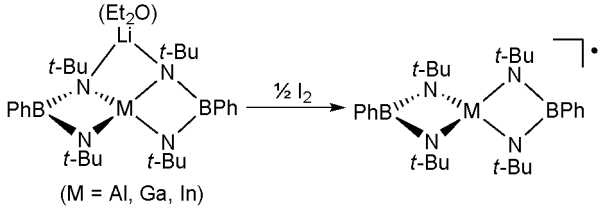

The corresponding boron and indium-containing radicals $\{M[PhB(\mu\text{-}N\text{-}t\text{-}Bu)_2]_2\}^{\bullet}$ (M = B, In) were characterized in solution by EPR spectroscopy (5). However, the green indium-containing radical is not sufficiently stable to be isolated in the solid state. The boron analogue, although it is thermally very stable, could not be obtained in a pure form owing to the formation of other products via a competing reaction pathway (5). Thallium(I) mono-*bam* complexes have also been structurally characterized; they form aggregated chains incorporating metallophilic Tl···Tl interactions in the solid state (6).

The synthesis and characterization of the group 13 complexes $\{M[PhB(\mu\text{-}N\text{-}t\text{-}Bu)_2]_2\}^{\bullet}$ (M = Al, Ga, In) raises the question of whether the isoelectronic group 14 cation radicals $\{M[PhB(\mu\text{-}N\text{-}t\text{-}Bu)_2]_2\}^{\bullet+}$ (M = Si, Ge, Sn) will be accessible by mild oxidation of the corresponding neutral precursors. Several *bam* complexes of group 14 elements (Si, Ge, Sn, Pb) have been reported (1). Although the metathesis reactions of two equivalents of Li_2*bam* reagents with MCl_4 (M = Ge, Sn) afford the corresponding M(*bam*)$_2$ complexes (7, 8), the synthesis of a silicon analogue (M = Si) by this method has not been reported. The known silicon complexes have only one *bam* ligand chelated to silicon in complexes of the type RR′Si(*bam*); they were prepared by indirect approaches rather than metathesis (9, 10). The solid-state structures of M(*bam*)$_2$ complexes (M = Ge, Sn) have not been determined. Interestingly, the reaction of $Li_2[PhB(\mu\text{-}N\text{-}t\text{-}Bu)_2]$ with $PbCl_4$ produces the dimeric lead(II) complex $\{Pb[PhB(\mu_3\text{-}N\text{-}t\text{-}Bu)_2]\}_2$, which is preferably prepared by using $PbCl_2$ as a source of lead(II) (11). There are no reports of complexes in which two *bam* ligands are chelated to a group 14 metal in the formal +2 oxidation state, i.e. $[M(bam)_2]^{2-}$ (M = Ge, Sn, Pb). These dianions are isoelectronic with the corresponding group 15 monoanions of the type $[M(bam)_2]^-$ (M = As, Sb, Bi), which exhibit interesting polycyclic structures in the solid state and fluctional behaviour in solution (12). The synthesis of dilithio derivatives of the group 14 dianions $[M(bam)_2]^{2-}$ (M = Ge, Sn, Pb) is, therefore, of interest for comparison with their group 15 analogues.

In this contribution we report (a) the X-ray structures of the complexes $M[PhB(\mu\text{-}N\text{-}t\text{-}Bu)_2]_2$ (**1a**, M = Ge; **1b**, M = Sn), (b) oxidation of **1b** with SO_2Cl_2 to give the radical cation $\{Sn[PhB(\mu\text{-}N\text{-}t\text{-}Bu)_2]_2\}^{\bullet+}$, which was identified by EPR spectroscopy supported by DFT calculations, (c) the synthesis and X-ray structures of the new heterotrimetallic complexes $Li_2Sn[PhB(\mu\text{-}N\text{-}t\text{-}Bu)_2]_2$ (**2b**) and $(THF{\cdot}Li)LiPb[PhB(\mu\text{-}N\text{-}t\text{-}Bu)_2]_2$ (**2c**·THF), and (d) variable temperature, multinuclear (^1H, ^{13}C, ^7Li, ^{11}B and ^{119}Sn) NMR investigations of the fluctional behaviour of **2b**.

Experimental section

Reagents and general procedures

All reactions and the manipulations of products were performed under an argon atmosphere by using standard Schlenk techniques or an inert atmosphere glove box. The compounds $PhBCl_2$ (Aldrich, 97%), $GeCl_4$ (Strem, 99.99%), $C_4H_8O_2{\cdot}GeCl_2$ (Aldrich, 99%), $SnCl_4$ (Aldrich, 1.0 M sol. in heptane), $SnCl_2$ (Aldrich, 98%), PbI_2 (Strem, 99.999%) and *t*-$BuNH_2$ (Aldrich, 98%) were used as received. SO_2Cl_2 (Aldrich, 97%) was distilled prior to use. LiN(H)-*t*-Bu was prepared by the addition of *n*-BuLi to a solution of anhydrous *t*-$BuNH_2$ in *n*-hexane at -10 ^oC and its purity was checked by ^1H NMR spectroscopy. The compounds $PhB[N(H)\text{-}t\text{-}Bu]_2$ and $Li_2[PhB(\mu\text{-}N\text{-}t\text{-}Bu)_2]$ were prepared as described earlier (13). The solvents *n*-hexane, toluene, Et_2O and THF were dried by distillation over Na/benzophenone under an argon atmosphere prior to use. Elemental analyses were performed by Analytical Services, Department of Chemistry, University of Calgary.

Spectroscopic methods

The ^1H, ^7Li, ^{11}B, ^{13}C and ^{119}Sn NMR spectra were obtained in d_8-toluene at 23 ^oC on a Bruker DRX 400 spectrometer operating at 399.59, 155.30, 128.20, 100.49 and 149.00 MHz, respectively. ^1H and ^{13}C spectra are referenced to the solvent signal and the chemical shifts are reported relative to $(CH_3)_4Si$. ^7Li and ^{11}B NMR spectra are referenced externally and the chemical

shifts are reported relative to a 1.0 M solution of LiCl in D_2O and to a solution of $BF_3{\cdot}Et_2O$ in C_6D_6, respectively. Similarly, the ^{119}Sn NMR spectra are referenced externally and the chemical shifts are reported relative to $(CH_3)_4Sn$.

The X-band EPR spectra were recorded on a Bruker EMX 113 spectrometer equipped with a variable-temperature accessory. EPR spectral simulations were carried out by using WINEPR *SimFonia* (version 1.25, 1996) and PEST *WinSim* (version 0.98, 2002) softwares (14).

X-ray crystallography

Crystallographic data for **1a**, **1b**, **2b** and **2c**·THF are summarized in Table 1.[4] Crystals of Ge[PhB(μ-N-*t*-Bu)$_2$]$_2$ (**1a**), Sn[PhB(μ-N-*t*-Bu)$_2$]$_2$ (**1b**), Li_2Sn[PhB(μ-N-*t*-Bu)$_2$]$_2$ (**2b**) and (THF·Li)LiPb[PhB(μ-N-*t*-Bu)$_2$]$_2$ (**2c**·THF) were coated with Paratone 8277 oil and mounted on a glass fibre. Diffraction data were collected on a Nonius KappaCCD diffractometer using monochromated MoK_α radiation (λ = 0.71073 Å) at -100 °C. The data sets were corrected for Lorentz and polarization effects, and empirical absorption correction was applied to the net intensities. The structures were solved by direct methods using SHELXS-97 (15) and refined using SHELXL-97 (16). After full-matrix least-squares refinement of the non-hydrogen atoms with anisotropic thermal parameters, the hydrogen atoms were placed in calculated positions [C-H = 0.98 Å for $C(CH_3)_3$ and 0.95 Å for phenyl hydrogens]. The isotropic thermal parameters of the hydrogen atoms were fixed at 1.2 times to that of the corresponding carbon for phenyl hydrogens, and 1.5 times for $C(CH_3)_3$. In the final refinement the hydrogen atoms were riding on their respective carbon atoms.

In the structure of **2b**, the Li2 and Sn1 atoms were disordered with the atoms statistically distributed over the two atomic sites. The two atoms were constrained to locate in the same position and the anisotropic thermal parameters were restricted to be equal. In the final refinement, the site occupation factors were *ca.* 93 and 7%, respectively. The scattering factors for the neutral atoms

were those incorporated with the programmes.

Computational Details

All calculations were done with the Gaussian 03 program using density functional theory (17). Molecular structures were optimized using the hybrid PBE1PBE exchange-correlation functional (18) together with the Ahlrichs' TZVP basis sets (19); an effective core potential basis set of similar valence quality was used for the heavy tin nuclei (20). Hyperfine coupling constants were then calculated by single-point calculations employing the optimized geometries and the basis set combination used for optimizations. The orbital plot was obtained by the program gOpenMol (21).

Synthesis of Ge[PhB(μ-N-*t*-Bu)$_2$]$_2$ (1a)

A solution of Li_2[PhB(μ-N-*t*-Bu)$_2$] (0.366 g, 1.50 mmol) in 30 mL of diethyl ether was added to a solution of $GeCl_4$ (0.161 g, 0.75 mmol) in 30 mL of diethyl ether at -80 ºC. The reaction mixture was allowed to reach room temperature in 30 min and it was then heated to 35 ºC for 15 h. The precipitate of LiCl was removed by filtration and the solvent was evaporated under vacuum giving Ge[PhB(μ-N-*t*-Bu)$_2$]$_2$ (**1a**) as a white powder (0.442 g, 83%). $C_{28}H_{46}B_2N_4Ge$: C 63.10; H 8.70; N 10.51. Found: C 62.85; H 8.94; N 10.71. ^{1}H NMR (d_8-toluene, 23 ºC): δ 7.20-7.49 [m, 10H, C_6H_5], 1.30 [s, 36H, C(CH_3)$_3$]. ^{13}C NMR: δ 139.1-126.7 [C_6H_5], 51.3 [s, *C*(CH$_3$)$_3$], 33.7 [s, *C*(*C*H$_3$)$_3$]. ^{11}B NMR: δ 35.2. Crystallization from *n*-hexane afforded colourless X-ray quality crystals of Ge[PhB(μ-N-*t*-Bu)$_2$]$_2$ (**1a**).

Synthesis of Sn[PhB(μ-N-*t*-Bu)$_2$]$_2$ (1b)

A solution of Li_2[PhB(μ-N-*t*-Bu)$_2$] (0.244 g, 1.00 mmol) in 25 mL of diethyl ether was added to a solution of $SnCl_4$ (0.5 mL of a 1.0 M solution in heptane, 0.50 mmol) in 25 mL of diethyl

ether at -80 °C. The reaction mixture was stirred for 30 min at -80 °C and 6 h at 23 °C. The precipitate of LiCl was removed by filtration and the solvent was evaporated under vacuum giving Sn[PhB(μ-N-*t*-Bu)$_2$]$_2$ (**1b**) as a white powder (0.257 g, 87%). $C_{28}H_{46}B_2N_4Sn$: C 58.08; H 8.01; N 9.68. Found: C 58.30; H 7.93; N 9.03. ^{1}H NMR (d$_8$-toluene, 23 °C): δ 7.12-7.49 [m, 10H, C_6H_5], 1.23 [s, 36H, C(CH_3)$_3$]. ^{13}C NMR: δ 135.1-126.8 [C_6H_5], 51.7 [s, *C*(CH$_3$)$_3$], 35.0 [s, *C*(*C*H$_3$)$_3$]. ^{11}B NMR: δ 35.0. ^{119}Sn NMR: δ -83.0 (*cf.* -117.8 ppm for Sn[(2,4,6-^{i}Pr$_3$C$_6$H$_2$)B(μ-N-*t*-Bu)$_2$]$_2$ in CDCl$_3$) (8). Crystallization from *n*-hexane afforded colourless X-ray quality crystals of Sn[PhB(μ-N-*t*-Bu)$_2$]$_2$ (**1b**).

Oxidation of Sn[PhB(μ-N-*t*-Bu)$_2$]$_2$ (1b) with SO_2Cl_2

A solution of SO_2Cl_2 (0.040 mL, 0.067 g, 0.50 mmol) was dissolved in 10.0 mL of diethyl ether; 1.0 mL (0.05 mmol) of this solution was added to a solution of **1b** (0.058g, 0.10 mmol) in 80 mL of diethyl ether at -80 °C. The reaction mixture was allowed to warm up to *ca*. -40 °C at which point the colourless solution became bright blue and a small amount of white powder (LiCl) appeared. An aliquot of the reaction solution was used for EPR spectroscopic measurements. The remaining reaction solution was allowed to reach room temperature, which resulted in the decomposition of the paramagnetic species at *ca.* 0 °C as indicated by disappearance of the blue colour.

Synthesis of Li$_2$Sn[PhB(*μ*-N-*t*-Bu)$_2$]$_2$ (2b)

A solution of Li$_2$[PhB(μ-N-*t*-Bu)$_2$] (0.366 g, 1.50 mmol) in 25 mL of diethyl ether was added to a suspension of $SnCl_2$ (0.142 g, 0.75 mmol) in 25 mL of diethyl ether at -80 °C. The reaction mixture was stirred for 30 min at -80 °C and 5 h at 23 °C. The precipitate of LiCl was removed by filtration and the solvent was evaporated under vacuum. The product was then washed

with cold *n*-hexane (*ca.* 10 mL) to give **2b** as a white powder (0.364 g, 75%). Anal. Calcd for $C_{32}H_{56}B_2Li_2N_4Sn$: C 56.72; H 7.82; N 9.45. Found: C 55.45; H 7.99; N 9.18. ^{1}H NMR (d_8-toluene, 23 °C): δ 6.98-7.72 [m, 10H, C_6H_5], 1.39 [shoulder, br, 9H, C(CH_3)$_3$], 1.19 [s, br, 27H, C(CH_3)$_3$]. ^{1}H NMR (0 °C): δ 6.96-7.72 [m, 10H, C_6H_5], 1.44 [s, 9H, C(CH_3)$_3$], 1.21 [s, 27H, C(CH_3)$_3$]. ^{1}H NMR (-20 °C): δ 6.92-7.70 [m, 10H, C_6H_5], 1.46 [s, 9H, C(CH_3)$_3$], 1.24 [s, 9H, C(CH_3)$_3$], 1.21 [s, 18H, C(CH_3)$_3$]. ^{13}C NMR (-20 °C): δ 133.9-125.8 [C_6H_5], 54.4 [s, *C*(CH$_3$)$_3$], 52.1 [s, *C*(CH$_3$)$_3$], 51.1 [s, *C*(CH$_3$)$_3$], 37.0 [s, C(*C*H$_3$)$_3$], 36.6 [s, *C*(*C*H$_3$)$_3$], 36.1 [s, C(*C*H$_3$)$_3$]. ^{11}B NMR (-20 °C): δ 36.6. ^{7}Li NMR (-20 °C): δ 1.10. ^{119}Sn NMR (d_8-toluene, 23 °C): δ -167.9 ppm. X-ray quality crystals of **2b** were obtained by dissolving the white powder in boiling *n*-hexane and then allowing the solution to cool down to room temperature in *ca.* 3 h.

Synthesis of (Et$_2$O·Li)LiPb[PhB(μ-N-*t*-Bu)$_2$]$_2$ (2c·OEt$_2$)

Method A. A solution of Li_2[PhB(μ-N-*t*-Bu)$_2$] (0.244 g, 1.00 mmol) in 30 mL of diethyl ether was added to a suspension of PbI_2 (0.231 g, 0.50 mmol) in 30 mL of diethyl ether at -80 °C. The reaction mixture was allowed to reach room temperature in 30 min and it was then heated to 35 °C for 12 h. The precipitate of LiI was removed by filtration and the solvent was evaporated under vacuum giving a pale yellow, amorphous powder (0.294 g). ^{1}H NMR spectroscopy revealed a mixture of products among which the lead(II) complex, {Pb[PhB(μ-N-*t*-Bu)$_2$]}$_2$, was identified (δ 1.15 ppm, d_8-toluene, 23 °C; lit. value (11): δ 1.19 in C_6D_6) in addition to the resonances of **2c**·OEt$_2$ (see discussion of the VT NMR experiments). **2c**·OEt$_2$: ^{1}H NMR (d_8-toluene, 23 °C): δ 7.02-7.78 [m, C_6H_5], 3.40 [q, 6H, (CH$_3$CH_2)$_2$O], 1.27 [s, br, 36H, C(CH_3)$_3$], 1.00 [t, 6H, (CH_3CH$_2$)$_2$O]. ^{1}H NMR (0 °C): δ 7.08-7.82 [m, C_6H_5], 3.34 [q, 6H, (CH$_3$CH_2)$_2$O], 1.35 [shoulder, 9H, C(CH_3)$_3$], 1.29 [s, 18H, C(CH_3)$_3$], 1.25 [shoulder, 9H, C(CH_3)$_3$], 0.97 [t, 6H, (CH_3CH$_2$)$_2$O]. ^{1}H NMR (-10 °C): δ 7.10-7.83 [m, C_6H_5], 3.34 [q, 6H, (CH$_3$CH_2)$_2$O], 1.36 [s, 9H, C(CH_3)$_3$], 1.30 [s, 18H, C(CH_3)$_3$], 1.25

[s, 9H, C(C*H*$_3$)$_3$], 0.96 [t, 6H, (C*H*$_3$CH$_2$)$_2$O]. ^{7}Li NMR (-20 ^{o}C): δ 0.87. Crystallization from THF afforded a few colourless crystals of (THF·Li)LiPb[PhB(μ-N-*t*-Bu)$_2$]$_2$ (**2c**·THF).

Method B. The Pb(II) complex {Pb[PhB(μ$_3$-N-*t*-Bu)$_2$]}$_2$ was prepared by a modification of the procedure reported earlier (11) from the reaction of PbI_2 (0.461 g, 1.00 mmol) and Li_2[PhB(μ-N-*t*-Bu)$_2$] (0.244 g, 1.00 mmol) in diethyl ether. The purity of the compound was checked by ^{1}H NMR spectroscopy. A solution of Li_2[PhB(μ-N-*t*-Bu)$_2$] (0.244 g, 1.00 mmol) in 30 ml of diethyl ether was added to a solution of {Pb[PhB(μ$_3$-N-*t*-Bu)$_2$]}$_2$ (0.437 g, 0.50 mmol) in 30 mL of diethyl ether at -80 ^{o}C. The reaction mixture was allowed to reach room temperature in 30 min and it was then heated to 35 ^{o}C for 18 h. The precipitate of LiI was removed by filtration and the solvent was evaporated under vacuum giving a pale yellow, amorphous powder (0.546 g). The ^{1}H NMR spectrum of this powder in d$_8$-toluene revealed a complex mixture of products. The reactions described in methods **A** and **B** were also carried out in THF at 55 ^{o}C without significant improvement in the yield of **2c**.

Reaction of Li_2[PhB(μ-N-*t*-Bu)$_2$] with $C_4H_8O_2$·$GeCl_2$

A solution of Li_2[PhB(μ-N-*t*-Bu)$_2$] (0.183 g, 0.75 mmol) in 25 mL of diethyl ether was added to a solution of $C_4H_8O_2$·$GeCl_2$ (0.174 g, 0.75 mmol) in 25 mL of diethyl ether at -80 ^{o}C. The reaction mixture was stirred for 30 min at -80 ^{o}C and 16 h at 23 ^{o}C. The precipitate of LiCl was removed by filtration and the solvent was evaporated under vacuum giving a pale yellow, amorphous powder (0.185g, 78% calculated as a 1:2 mixture of **1a** and {Ge[PhB(μ-N-*t*-Bu)$_2$]}$_2$, see discussion). ^{1}H NMR (d$_8$-toluene, 23 ^{o}C): δ 7.02-7.96 [m, 30H, C$_6$*H*$_5$], 1.41 [s, 36H, C(C*H*$_3$)$_3$], 1.39 [s, 36H, C(C*H*$_3$)$_3$], 1.30 [s, 36H, C(C*H*$_3$)$_3$]. ^{11}B NMR (-20 ^{o}C): δ *ca.* 36.5 (br). Crystallization from *n*-hexane afforded a few colourless crystals of Ge[PhB(*μ*-N-*t*-Bu)$_2$]$_2$ (**1a**).

Results and discussion

X-ray structures of M[PhB(μ-N-*t*-Bu)$_2$]$_2$ (1a, M = Ge; 1b, M = Sn)

The germanium(IV) and tin(IV) complexes **1a** and **1b** were obtained in excellent yields (*ca*. 85 %) by a modification of the literature synthesis in which the dilithium reagent Li$_2$[PhB(μ-N-*t*-Bu)$_2$] was isolated and purified prior to reaction with MCl_4 (M = Ge, Sn) in a 2:1 molar ratio in diethyl ether. The NMR spectroscopic data (see Experimental Section) showed minor variations compared with the literature values (7). Attempts to make the silicon analogue Si[PhB(μ-N-*t*-Bu)$_2$]$_2$ by a similar procedure were unsuccessful.

The X-ray structural determinations of **1a** and **1b** confirmed the expected spirocyclic structures with two orthogonal *bam* ligands *N,N′*-chelated to the distorted tetrahedral metal centres (Fig. 1). In both complexes the molecule lies on a crystallographic two-fold axis that imposes equivalence on the two *bam* ligands. The diamagnetic complexes **1a** and **1b** are isostructural with the paramagnetic group 13 analogues {M[PhB(μ-N-*t*-Bu)$_2$]$_2$}$^{\bullet}$ (M = Al, Ga) (4). The centrosymmetric germanium(IV) complex **1a** represents the first structurally characterized germanium *bam* complex (1).

Selected bond lengths and bond angles for **1a** and **1b** are summarized in Table 2. The distorted tetrahedral germanium centre in **1a** exhibits equal Ge-N bond lengths, which are noticeably shorter (by *ca.* 0.20 Å) than the corresponding M-N bonds in the heavier tin analogue **1b**. Somewhat surprisingly, the Ge-N bonds in **1a** are also significantly shorter than the Ga-N bond lengths of 1.922(2) Å observed in the neutral radical Ga[PhB(μ-N-*t*-Bu)$_2$]$_2^{\bullet}$ (4), despite the difference of only one electron between the two centres (Ge and Ga). The Ge-N bond lengths are, however, equal within estimated standard deviation with the Al-N bond lengths of 1.842(2) and 1.852(2) Å reported for {Al[PhB(μ-N-*t*-Bu)$_2$]$_2$}$^{\bullet}$ (4), for which the difference between the two metal centers (Ge and Al) is nine electrons. These trends in bond lengths may be attributed to the weaker Coulomb interaction in the paramagnetic group 13 complexes where the total charge on the ligands is formally 3-

compared to the diamagnetic group 14 complexes for which the formal charge is 4-. Interestingly, the Ge-N bonds in **1a** are also *ca.* 0.04 Å longer than the As-N bond lengths of 1.797(4)-1.811(4) Å observed in the isostructural, and *isoelectronic*, group 15 cation $As[PhB(\mu\text{-}N\text{-}t\text{-}Bu)_2]_2^+$ (in the $GaCl_4^-$ salt) (22). Since the single bond covalent radius is the same for Ge and As (1.22 Å) (23), the shorter As-N bonds are probably due to the stronger electrostatic interaction between the positively charged arsenic centre and the two dianionic *bam* ligands. In the tin(IV) complex **1b** the Sn-N bonds within each *bam* ligand are equal in length and are close to the values of 2.043(3)-2.066(3) Å observed in the eight-membered rings $\{Me_2Sn[\mu\text{-}N(Me)B(R)NMe]_2SnMe_2\}$ (R = 2,4,6-*i*-$Pr_3C_6H_2$, 2,4,6-*t*-$Bu_3C_6H_2$), which also involve Sn(IV) centres (8, 24), but they are somewhat shorter than the value of 2.105(1) Å found for the Sn-N bond involving a three-coordinate nitrogen atom in the dimeric Sn(II) complex, $\{Sn[MeB(\mu\text{-}NSiMe_3)_2]\}_2$ (25). The B-N bond lengths in both **1a** and **1b** are equal and represent typical values for the *bam* ligand (1).

The M-N-B angles in **1a** and **1b** are close to 90° and the geometry about boron atom is trigonal planar as indicated by the sum of bond angles (360°). The N-B-N and all N-Ge-N angles in **1a** are close to the corresponding bond angles observed in $\{Al[PhB(\mu\text{-}N\text{-}t\text{-}Bu)_2]_2\}^{\bullet}$ (4) due to the identical Ge-N/Al-N and B-N bond lengths, whereas the longer Sn-N bonds result in a narrower N-Sn-N angle by *ca.* 7 and 3° within the *bam* ligands in **1b**. The $GeBN_2$ four-membered rings in **1a** are planar with torsion angles of 0.5(2) and 0.6(2)° for ∠ N2-Ge1-N1-B1 and Ge1-N1-B1-N2, respectively, while the corresponding torsion angles for the slightly puckered $SnBN_2$ four-membered rings in **1b** are 4.6(2) and 6.5(3)°.

Although all four isostructural compounds (**1a**, **1b** and $M[PhB(\mu\text{-}N\text{-}t\text{-}Bu)_2]_2^{\bullet}$ (M = Al, Ga)) exhibit a centre of symmetry at the group 13 or 14 atom, the tin complex **1b** exhibits different crystal packing from the other three complexes as indicated by the crystal system and space group [monoclinic *C*2/*c* for **1b** *vs.* orthorhombic *Pbcn* for **1a** and $M[PhB(\mu\text{-}N\text{-}t\text{-}Bu)_2]_2^{\bullet}$ (M = Al, Ga)].

EPR spectra and DFT calculations of the radical cation $\{Sn[PhB(\mu\text{-}N\text{-}t\text{-}Bu)_2]_2\}^{\bullet+}$

The intensely coloured spirocyclic group 13 radicals $\{M[PhB(\mu\text{-}N\text{-}t\text{-}Bu)_2]_2\}^{\bullet}$ (M = Al, Ga) (Scheme 1) are stable in the solid state (4), while the indium analogue $\{In[PhB(\mu\text{-}N\text{-}t\text{-}Bu)_2]_2\}^{\bullet}$ has only been characterized in solution by EPR spectroscopy (5). In an attempt to generate the isoelectronic radical cations with a group 14 metal centre, $\{M[PhB(\mu\text{-}N\text{-}t\text{-}Bu)_2]_2\}^{\bullet+}$ (M = Ge, Sn), we have investigated the reactions of **1a** and **1b** with various oxidizing agents (Scheme 2).

Scheme 2. One-electron oxidation of $\{M[PhB(\mu\text{-}N\text{-}t\text{-}Bu)_2]_2\}$ (M = Ge, Sn)

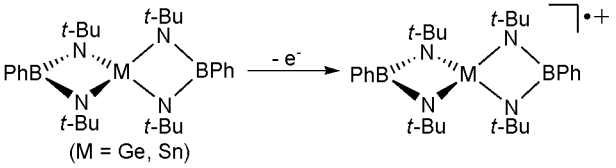

The attempted one-electron oxidation of **1a** or **1b** to the corresponding radical cation by one-half equivalent of I_2 in diethyl ether or THF resulted in no reaction even at elevated temperatures. The tin(IV) complex **1b** was also inert towards $[NO][SbF_6]$ and, surprisingly, the germanium(IV) complex **1a** showed no indication of a reaction with SO_2Cl_2. However, the treatment of **1b** with one-half equivalent of SO_2Cl_2 in diethyl ether at low temperatures produced a bright blue solution of $\{Sn[PhB(\mu\text{-}N\text{-}t\text{-}Bu)_2]_2\}^{\bullet+}$ (*vide infra*), which was persistent below -40 ^{o}C, but decomposed above 0 ^{o}C, *cf.* the thermal instability of the isoelectronic indium-containing neutral radical $\{In[PhB(\mu\text{-}N\text{-}t\text{-}Bu)_2]_2\}^{\bullet}$ (5).

The EPR spectrum of the blue solution in diethyl ether displays an eight-line pattern and a highly broadened lineshape (Fig. 2); the g-value of this radical is 2.0055. Several attempts to resolve additional fine structure in the EPR spectrum by variations in the solvent, concentration of the solution and temperature, as well as changes in the measurement parameters, were unsuccessful. A reasonable simulation of the observed spectrum is obtained by using a line width of 2.85 G (95%

Gaussian shape) and by including hyperfine coupling constants to one boron atom (^{11}B, I = 3/2, 9.88 G) and two equivalent nitrogen centers (^{14}N, I = 1, 9.18 G) (Fig. 2) thus suggesting localization of the unpaired electron in only one of the *bam* units, in contrast to the delocalization over both *bam* ligands observed for the neutral group 13 radicals {M[PhB(μ-N-*t*-Bu)$_2$]$_2$}$^\bullet$ (M = Al, Ga, In) (4, 5). This electron distribution is, however, reminiscent of the behaviour noted for the persistent radicals {(Et$_2$O)Li[PhB(μ-N-*t*-Bu)$_2$]$_2$M}$^\bullet$ (M = Mg, Zn), which exhibit localization of the unpaired electron on the spin-active nuclei in only one of the *bam* ligands as a consequence of the coordination of the additional lithium counter-cation to the second *bam* unit (5).

The apparent localization of the unpaired electron in only one of the *bam* ligands, and the strong coordinating nature of the Cl^- counter-anion, raised the possibility of the formation of neutral radicals, {Sn[PhB(μ-N-*t*-Bu)$_2$]$_2$Cl}$^\bullet$, comprising a Sn-Cl or B-Cl contact instead of the ion-separated radical cation, {Sn[PhB(μ-N-*t*-Bu)$_2$]$_2$}$^{\bullet+}$ (Scheme 3), *cf.* the Zwitterionic arsenic(V) complex, {[PhB(μ-N-*t*-Bu)$_2$]As[(μ-N-*t*-Bu)$_2$B(Cl)Ph]}, with a covalent B-Cl bond (22). Consequently, the replacement of the Cl^- anion by the weakly coordinating SbF_6^- was performed by an *in situ* reaction with $AgSbF_6$. The thermal stability of the radical cation was not improved, but a colour change from blue to purple was observed along with the formation of AgCl. The EPR spectrum of the purple solution, however, was unaffected by the change of the counter-anion, suggesting that the one-electron oxidation product of **1b** is present *in very dilute diethyl ether solutions* as the ion-separated radical cation **I** rather than the "contact ion-pairs" **II** or **III**.

Scheme 3. Possible structures of the product of one-electron oxidation of **1b** with SO_2Cl_2.

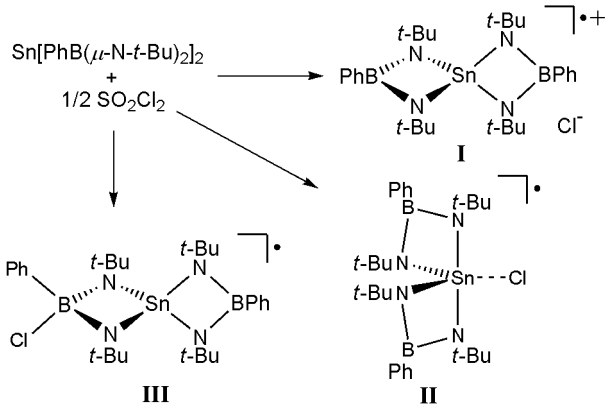

Density functional theory calculations conducted for the cation radical {Sn[PhB(μ-N-*t*-Bu)$_2$]$_2$}$^{\bullet+}$ predict a C_{2v}-symmetric minimum structure and localized spin density on only one *bam*-ligand (Fig. 3). A D_{2d}-symmetric structure, analogous to that observed for the neutral group 13 radicals {M[PhB(μ-N-*t*-Bu)$_2$]$_2$}$^{\bullet}$ (M = Al, Ga) (Scheme 1), is a transition state with respect to Sn-N stretching vibrations and only 5 kJ mol^{-1} higher in energy. Hence, it appears that the spiroconjugative interactions in **1b** are not sufficiently strong to give rise to a fully delocalized electron distribution in the corresponding cation,[5] and the system adopts a structure with the two *bam*-ligands bearing different formal charges, i.e. Sn(IV)(*bam*)$^{2-}$(*bam*)$^{-\bullet}$. This is consistent with the finding that optimizations carried out for the lighter group 14 congeners of {M[PhB(μ-N-*t*-Bu)$_2$]$_2$}$^{\bullet+}$ (M = Si, Ge) give minima with significantly shorter N···N separations and, consequently, only D_{2d}-symmetric structures are found.

The hyperfine coupling constants calculated for Sn[PhB(μ-N-*t*-Bu)$_2$]$_2$}$^{\bullet+}$ (2 × ^{14}N, 7.35 G; 2 × ^{14}N, 0.05 G; ^{11}B, -10.96 G; ^{11}B, -0.32 G) are in good agreement with the values determined from the experimental spectrum. Similar to the previous observations for the persistent radicals {(Et$_2$O)Li[PhB(*μ*-N-*t*-Bu)$_2$]$_2$M}$^{\bullet}$ (M = Mg, Zn) (5), the calculated nitrogen couplings are too small, whereas the coupling to the boron nuclei is slightly larger than the value inferred from the simulation; there is an apparent tendency of this functional basis set combination to underestimate

couplings that result from the spin density of the unpaired electron while overestimating those which arise from spin-polarization effects (4, 5). The undulating baseline of the EPR spectrum and the low intensity humps visible at both ends of the spectrum most likely arise from the presence of small amounts of isotopomers which contain the spin-active tin nuclei (^{117}Sn, I = ½, 7.6 %; ^{119}Sn, I = ½, 8.6 %). The magnitudes of the two Sn couplings cannot, however, be obtained with the current computational method due to the indirect treatment of relativistic effects via effective core potential basis sets. The observed broad lineshape can, at least in part, be attributed to the numerous smaller couplings to the hydrogen atoms of the *t*-Bu groups.[6]

Synthesis of $Li_2Sn[PhB(\mu\text{-}N\text{-}t\text{-}Bu)_2]_2$ (2b) and $(THF{\cdot}Li)LiPb[PhB(\mu\text{-}N\text{-}t\text{-}Bu)_2]_2$ (2c·THF)

The reactions of $Li_2[PhB(\mu\text{-}N\text{-}t\text{-}Bu)_2]$ with group 14 dihalides in a 2:1 molar ratio were investigated with a view to isolating and structurally characterizing complexes of the type $Li_2M[PhB(\mu\text{-}N\text{-}t\text{-}Bu)_2]_2$ in which the dianions $M[PhB(\mu\text{-}N\text{-}t\text{-}Bu)_2]_2^{2-}$ (M = Ge, Sn, Pb) are isoelectronic with the previously reported group 15 anions $M[PhB(\mu\text{-}N\text{-}t\text{-}Bu)_2]_2^{-}$ (M = As, Sb, Bi), which were obtained as monolithium derivatives (12). The outcome of these reactions was markedly dependent on the nature of the group 14 metal.

The reaction between $Li_2[PhB(\mu\text{-}N\text{-}t\text{-}Bu)_2]$ and $SnCl_2$ in a 2:1 molar ratio in diethyl ether proceeded cleanly to produce $Li_2Sn[PhB(\mu\text{-}N\text{-}t\text{-}Bu)_2]_2$ (**2b**) in 75 % yield (eq. [1]). The unsolvated heterotrinuclear complex **2b** was characterized in solution by multinuclear NMR spectroscopy and in the solid state by single crystal X-ray crystallography.

[1] $2\ Li_2[PhB(\mu\text{-}N\text{-}t\text{-}Bu)_2] + SnCl_2 \rightarrow Li_2Sn[PhB(\mu\text{-}N\text{-}t\text{-}Bu)_2]_2 + 2\ LiCl$

(**2b**)

The reaction of $Li_2[PhB(\mu\text{-N-}t\text{-Bu})_2]$ with PbI_2 in 2:1 molar ratio was conducted under various conditions in an effort to produce the analogous lead(II) complex $Li_2Pb[PhB(\mu\text{-N-}t\text{-Bu})_2]_2$ (**2c**). The ^{1}H NMR spectrum of the reaction mixture, however, revealed several products, one of which was identified as the previously reported mononuclear lead(II) complex, $\{Pb[PhB(\mu_3\text{-N-}t\text{-Bu})_2]\}_2$ (11). In an alternative synthetic approach, this dimeric Pb(II) complex was prepared and isolated prior to treatment with two equivalents of $Li_2[PhB(\mu\text{-N-}t\text{-Bu})_2]$. However, this two-step method also afforded a mixture of products from which only a few crystals of **2c** were isolated as the tetrahydrofuran solvate, $(THF\cdot Li)LiPb[PhB(\mu\text{-N-}t\text{-Bu})_2]_2$ (**2c**·THF).

The reaction of $Li_2[PhB(\mu\text{-N-}t\text{-Bu})_2]$ with $C_4H_8O_2\cdot GeCl_2$ in 2:1 molar ratio in diethyl ether produced several products (^{1}H NMR). Consequently, the reaction was repeated in 1:1 molar ratio in an attempt to form the unknown germanium(II) complex, $Ge[PhB(\mu\text{-N-}t\text{-Bu})_2]$, for subsequent reaction with $Li_2[PhB(\mu\text{-N-}t\text{-Bu})_2]$; this two-step approach was previously found to be necessary for the successful synthesis of the aluminum complex $(Et_2O\cdot Li)Al[PhB(\mu\text{-N-}t\text{-Bu})_2]_2$ (4). The ^{1}H NMR spectrum of the product(s) showed three equally intense resonances for N-*t*-Bu -groups at 1.41, 1.39 and 1.30 ppm (d_8-toluene, 23 ^{o}C). The chemical shift of 1.30 ppm is identical with the value observed for the *t*-Bu groups in the germanium(IV) complex $Ge[PhB(\mu\text{N-}t\text{-Bu})_2]_2$ (**1a**) (8), suggesting that a redox process has occurred. The resonances at 1.41 and 1.39 are tentatively assigned to the *t*-Bu groups attached to the three- and four-coordinate nitrogen atoms of the dimeric complex germanium(II) complex $\{Ge[PhB(\mu\text{-N-}t\text{-Bu})_2]\}_2$; however, attempts to isolate this second product were unsuccessful.

X-ray structures of $Li_2Sn[PhB(\mu\text{-N-}t\text{-Bu})_2]_2$ (2b) and $(THF\cdot Li)LiPb[PhB(\mu\text{-N-}t\text{-Bu})_2]_2$ (2c·THF)

Crystals of **2b** and **2c**·THF were obtained by recrystallization from boiling n-hexane and THF, respectively.[7] The crystal structures of **2b** and **2c**·THF with the atomic numbering scheme are depicted in Fig. 4 and the pertinent bond parameters are summarized in Table 3. The structures

reveal novel polycyclic arrangements, which bear a close similarity with each other despite the introduction of a solvent molecule in **2c**·THF. In both frameworks one of the *bam* ligands is *N,N′*-chelated to both the M(II) atom (M = Sn, Pb) and one of the Li^+ ions while the second *bam* ligand exhibits a unique bonding motif by bridging all three metal centers (1). While one of the Li^+ ions (Li1) in both structures is coordinated to three nitrogens, the second lithium in **2c**·THF is coordinated to two nitrogen atoms and the solvent molecule. The absence of the solvent molecule in **2b** affords a third, albeit relatively weak, Li···N close contact [2.557(6) Å] for the second lithium cation that results in a formal coordination number of five for the N4 atom (Fig. 4a).

Lithium salts of the group 15 monoanions $M[PhB(\mu\text{-}N\text{-}t\text{-}Bu)_2]_2^-$ (**3**, M = Sb; **4**, M = Bi) (12), which are isoelectronic with the group 14 dianions $M[PhB(\mu\text{-}N\text{-}t\text{-}Bu)_2]_2^{2-}$ (M = Sn, Pb), provide an interesting benchmark for comparison with the structures of **2b** and **2c**·THF (Scheme 4) Curiously, the lighter complexes in both group 14 (M = Sn) and group 15 (M = Sb) seem to favour unsolvated structures, whereas solvation of the Li^+ cation is observed for the heavier congeners (M = Pb, Bi). The molecular structure of the antimony complex **3** is comprised of two four-membered rings, BN_2Li and BN_2Sb, connected by Li-N and Sb-N bonds to form a tricyclic compound with both three and four-coordinate nitrogens (12). The introduction of a second Li^+ ion in **2b** has a surprisingly small effect on the overall structure; the molecule retains the ladder-like backbone and *cisoid* arrangement of the PhBN-*t*-Bu -units. Most significantly, however, the Li2···N4 contact in **2b** (Fig. 4a, dashed line in Scheme 4) is elongated by *ca.* 0.28 Å compared to the analogous bond in the antimony complex due to the *pseudo*-five-coordination of the nitrogen atom. The lithium cation in the bismuth complex **4**·OEt_2 (Scheme 4) is four-coordinate, being *N,N′*-chelated by one *bam* ligand and bonded to one nitrogen of the second *bam* ligand; the fourth coordination site is occupied by a Et_2O molecule (12). The introduction of a second Li^+ ion in **2c**·THF ruptures the bond between the solvated Li^+ ion and the second *bam* ligand, and cleaves the fourth M-N bond (M = Bi) that exists in the structure of **4**·OEt_2, although it is elongated compared to the other three Bi-N bonds (by *ca.* 0.18

Å) (12). As a result, both Li^+ ions are three-coordinate and all four nitrogen atoms are four-coordinate in **2c**·THF.

Scheme 4. Comparison of the structures of $Li_2M[PhB(\mu\text{-}N\text{-}t\text{-}Bu)_2]_2$ (M = Sn, Pb) and $LiM[PhB(\mu\text{-}N\text{-}t\text{-}Bu)_2]_2$ (M = Sb, Bi)

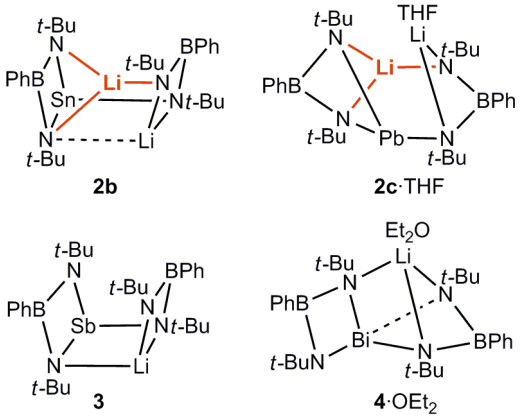

The average Sn-N bond length of 2.187(4) Å in **2b** (Fig. 4a, Table 3) is significantly longer than the values of 2.043(3)-2.066(3) Å observed in **1b** and in the Sn(IV) complexes $\{Me_2Sn[\mu\text{-}N(Me)B(R)NMe]_2SnMe_2\}$ (R = 2,4,6-*i*-$Pr_3C_6H_2$, 2,4,6-*t*-$Bu_3C_6H_2$) (8, 24), but slightly shorter than the distance of 2.254(13) Å found for the Sn-N bonds involving four-coordinate nitrogen atoms in the dimeric Sn(II) complex $\{Sn[MeB(\mu_3\text{-}NSiMe_3)_2]\}_2$ (25). Expectedly, the Sn-N bond lengths are also close to the values of 2.145(5) and 2.198(5) Å observed for the Sb-N bonds to the four-coordinate nitrogens in **3** (the single bond covalent radii for Sn and Sb are 1.40 and 1.43 Å, respectively) (23). The Li1-N distance to the bridging *bam* ligand is *ca.* 0.18 Å shorter than the two Li1-N bonds to the chelating *bam* ligand. To compensate for the long Li2···N4 contact, the two Li2-N bonds of 1.869(5) and 1.884(5) Å are among the shortest lithium-nitrogen bonds observed for this ligand system (1).

The introduction of a second Li^+ ion in **2b** results in opening the angle between BN_2Sn and LiN_2Sn four-membered rings as illustrated by the N1-Sn1-N3 and Li2-N4-B2 angles, which are *ca*. 4 and 9^o wider, respectively, than the corresponding angles in the related antimony complex, **3** (12). Widening of these angles and elongation of the Sn1-N1 and Li2-N4 contacts in **2b** compared to the analogous Sb-N and Li-N bonds, however, allows B1 and N2 atoms to incline towards the central $SnLiN_2$ four-membered ring and, consequently, the Sn1-N1-B1 and N4-Li2-N2 angles are *ca.* 4 and 5^o narrower than the comparable angles in **3**. The N-Sn-N angle within the chelating *bam* ligand in **2b** is *ca.* 5.7^o smaller than the corresponding angle in **1b** owing to the slightly longer Sn-N bonds in **2b**.

The average Pb-N bond length in **2c**·THF (Fig. 4b, Table 3) of 2.330(3) Å is identical to the value of 2.329(6) Å observed for the Pb-N bond involving a four-coordinate nitrogen atom in the dimeric lead(II) complex $\{Pb[PhB(\mu_3\text{-}N\text{-}t\text{-}Bu)_2]\}_2$ (10). The Pb-N bonds are *ca.* 0.06 Å longer than the three Bi-N bonds in **4**·OEt_2 (*cf*. the single bond covalent radii of 1.54 and 1.52 Å for Pb and Bi) (23), but they are *ca.* 0.11 Å shorter than the fourth, elongated, Bi-N bond in the bismuth complex (12). The Li-N distances to the N2 atom in the bridging ligand in **2c**·THF are somewhat shorter than the remaining three Li-N interactions (*ca.* 0.12 and 0.07 Å for Li1-N2 and Li2-N2, respectively). All these distances are consistent with, for example, those in the group 13 and 15 complexes $(Et_2O{\cdot}Li)M[PhB(\mu\text{-}N\text{-}t\text{-}Bu)_2]_2$, which show two (M = Ga, In, As) or three (M = Bi) Li-N interactions (3, 12). The N-Pb-N angle in the chelating ligand is *ca.* 10^o narrower than the N-Li-N angle at the unsolvated Li^+ ion due to the longer Pb-N bonds.

The bridging *bam* ligand in both **2b** and **2c**·THF exhibits a significant disparity in the B-N bond lengths (*ca*. 0.12 and 0.08 Å, respectively), presumably as a result of the different environments of N1 and N2, whereas the equality of the B-N bonds in the chelating *bam* ligand is not significantly perturbed by the weak Li2···N4 contact. The N-B-N angle in the chelating ligand in both **2b** and **2c**·THF is somewhat smaller (by 7.1 and 6.4^o, respectively) than the analogous bond

angle in the bridging *bam* ligand. Nevertheless, the boron atom assumes trigonal planar geometry in the *bam* ligands in both complexes**.** The bond angles at the nitrogen atoms in the chelating ligand are close to 90^{o}, whereas the loss of the fourth M-N bond results in a wider M1-N1-B1 angle by *ca.* 32^{o} (M = Sn) and 30^{o} (M = Pb).

NMR spectra and fluctional behaviour of $Li_2Sn[PhB(\mu\text{-}N\text{-}t\text{-}Bu)_2]_2$ (2b)

The ^{1}H NMR spectrum of **2b** in d_8-toluene at 23 ^{o}C exhibits a broad, poorly resolved signal for *t*-Bu groups, in addition to typical resonances for the phenyl groups. When the temperature is lowered to 0 ^{o}C, this broad resonance resolves into two well-separated signals at 1.44 and 1.21 ppm in a 1:3 intensity ratio. Cooling the solution to -20 ^{o}C results in resolution of the latter resonance to give three singlets at 1.46, 1.24 and 1.21 ppm in a 1:1:2 intensity ratio.[8] No further changes are apparent at lower temperatures. Consistently, the ^{13}C NMR spectrum of **2b** at -20 ^{o}C exhibits three singlets at 54.4, 52.1 and 51.1 ppm for the α-carbon atoms of the *t*-Bu groups; three singlets are also observed for the methyl carbons at 37.0, 36.6 and 36.1 ppm, in addition to the phenyl resonances. Throughout the temperature range (from -80 to +23 ^{o}C) only one broad singlet is observed in both the ^{11}B and ^{7}Li NMR spectrum (at 36.6 and 1.10 ppm, respectively, at -20 ^{o}C in d_8-toluene). The ^{119}Sn NMR spectrum of **2b** shows a single resonance at -167.9 ppm, which exhibits a significant shift to higher field from the value of 120 ppm reported for the dimeric tin(II) complex, $\{Sn[MeB(\mu_3\text{-}NSiMe_3)_2]\}_2$ (25). However, chemical shift values of -151.8 to -158.1 ppm have been reported for the related tin(II) complexes $\{Sn[RSi(\mu_3\text{-}N\text{-}t\text{-}Bu)_2]\}_2$ (R = C_3H_6, C_4H_6, C_4H_8 and C_5H_{10}) (26), which exhibit a coordination environment around the tin(II) centres similar to that in **2b**. The three resonances with a 1:1:2 intensity ratio observed at -20 ^{o}C in the ^{1}H NMR spectrum of **2b** are assigned to the *tert*-butyl groups attached to N1, N2 and N3/N4, respectively (Fig. 4a). The observation of only one broad resonance for the inequivalent boron and lithium atoms in the structure of **2b** even at low temperatures is attributed to overlap of these resonances.

The fluctional behaviour observed for **2b** is reminiscent of the exchange processes exhibited by the related group 15 complexes, **3** and **4**·OEt_2, which both showed only a single *t*-Bu resonance at room temperature (12). These types of fluctional processes in lithium derivatives of polyimido anions of p-block elements are known to have low activation energies (27). In the case of **3** and **4**·OEt_2, the fluctionality was determined to originate from a Berry pseudorotation (12). In a similar manner, the single resonance observed at room temperature in the ^{1}H NMR spectra of **2b** can be attributed to a rapid exchange in which each of the four nitrogens, in turn, occupy the site that is not coordinated to the tin centre.

Conclusions

Comparison of the properties of the cation radicals $\{M[PhB(\mu\text{-}N\text{-}t\text{-}Bu)_2]_2\}^{\bullet+}$ (M = Si, Ge, Sn) with those of the isoelectronic neutral radicals $M[PhB(\mu\text{-}N\text{-}t\text{-}Bu)_2]_2^{\bullet}$ (M = Al, Ga, In) was limited to the tin derivative as a result of the inertness of $Ge[PhB(\mu\text{-}N\text{-}t\text{-}Bu)_2]_2$ towards oxidizing agents and the inaccessibility of $Si[PhB(\mu\text{-}N\text{-}t\text{-}Bu)_2]_2$. The blue radical cation $\{Sn[PhB(\mu\text{-}N\text{-}t\text{-}Bu)_2]_2\}^{\bullet+}$, which exhibits thermal instability similar to that of the neutral group 13 analogue $In[PhB(\mu\text{-}N\text{-}t\text{-}Bu)_2]_2^{\bullet}$, was characterized at low temperatures by EPR spectroscopy. In contrast to the isoelectronic, D_{2d}-symmetric indium bis-*bam* radical, DFT calculations predict a C_{2v} symmetry for the radical cation $\{Sn[PhB(\mu\text{-}N\text{-}t\text{-}Bu)_2]_2\}^{\bullet+}$ with spin density localized on only one of the *bam* ligands owing to the weak spiroconjugative N···N interactions that, presumably, prevent the delocalization of the unpaired electron over both ligands.

In the heterotrimetallic complexes $Li_2M[PhB(\mu\text{-}N\text{-}t\text{-}Bu)_2]_2$ [M = Sn, Pb (THF omitted)], one of the *bam* ligands exhibits a novel bonding mode in which it bridges all three metal centres (1). The solid-state structures of these group 14 complexes are comparable with those of the previously reported group 15 complexes $LiM[PhB(\mu\text{-}N\text{-}t\text{-}Bu)_2]_2$ [M = Sb, Bi (OEt_2 omitted)] (12). Despite the introduction of a second Li^+ ion, the tin complex maintains the ladder-like backbone and *cisoid*

arrangement of the *bam* ligands found in the antimony analogue. The intrusion of a second Li^+ ion in the lead complex results in rupture of the bond between the solvated Li^+ ion and one of the *bam* ligands, as well as cleavage of the fourth M-N bond (M = Bi, Pb) that exists in the structure of $(Et_2O{\cdot}Li)Bi[PhB(\mu\text{-N-}t\text{-Bu})_2]_2$. In view of these structural similarities it is, perhaps, not surprising that the variable temperature NMR spectra of $Li_2Sn[PhB(\mu\text{-N-}t\text{-Bu})_2]_2$ show trends comparable to those previously observed for the group 15 complex $LiSb[PhB(\mu\text{-N-}t\text{-Bu})_2]_2$ (12), implying that the fluctional processes are also similar.

Acknowledgements

The authors gratefully acknowledge financial support from the Natural Sciences and Engineering Research Council (Canada) and the Academy of Finland. Prof. M. Balakrishna carried out a preliminary reaction of PbI_2 with $Li_2[PhB(\mu\text{-N-}t\text{-Bu})_2]$, which produced the crystals that were used in the X-ray structural determination of **2c**·THF.

Footnotes

[1] Department of Chemistry, University of Calgary, Calgary, Alberta T2N 1N4, Canada.

[2] Department of Chemistry, University of Jyväskylä, P.O. Box 35, Jyväskylä, FI-40014, Finland.

[3] Corresponding author (e-mail: chivers@ucalgary.ca).

[4] Supplementary data for this article are available on the journal Web site (canjchem.nrc.ca) or may be purchased from the Depository of Unpublished Data, Document Delivery, CISTI, National Research Council Canada, Ottawa, ON K1A 0R6, Canada. DUD 3672. For more information on obtaining material, refer to cisti-icist.nrc-cnrc.gc.ca/irm/unpub_e.shtml. CCDCXXXXXX-XXXXXX contain the crystallographic data for this article. These data can be obtained, free of charge, via www.ccdc.cam.ac.uk/conts/retrieving.html (or from the Cambridge Crystallographic Centre, 12 Union Road, Cambridge CB2 1EZ, UK; fax +44 1223 336033; or deposit@ccdc.cam.ac.uk).

[5] Spiroconjugation is thought to contribute to the stability of the neutral group 13 radicals {M[PhB(μ-N-*t*-Bu)$_2$]$_2$}$^\bullet$ (M = Al, Ga) (see ref. 4, and references cited therein).

[6] DFT calculations were also performed for the neutral (C_1 symmetric) systems **II** and **III** (Scheme 3), which comprise a Sn-Cl or a B-Cl bond, respectively. The paramagnetic species **II** is *ca*. 80 kJ mol^{-1} lower in energy, but the calculated hyperfine coupling constants for **II** and **III** are in poor agreement with those obtained from the experimental spectrum. The Sn-Cl bonded radical **II** exhibits a large (-11.56 G) coupling to the ^{11}B centre but, due to the lack of symmetry, the hfc couplings to the two nitrogen atoms are not equal (9.15 G and 5.56 G). The B-Cl bonded system **III** displays a coupling of -7.37 G to the ^{11}B isotope, and two inequivalent couplings of 11.24 and 2.26 G to the ^{14}N nuclei.

[7] Crystals of **2b** could not be obtained from diethyl ether. The attempted recrystallization of **2b** from THF resulted in a yellow solution, which contained the tin(IV) complex **1b** [^{1}H NMR spectrum (in d$_8$-THF)] as one component.

[8] The variable temperature ^{1}H NMR spectra of the lead complex **2c** exhibit similar trends; the broad singlet observed for *t*-Bu groups at 1.27 ppm at 23 ^{o}C resolves into three resonances at 1.36, 1.30 and 1.25 ppm (with a 1:2:1 intensity ratio) at -10 ^{o}C. However, these and other NMR data for **2c** were obtained on a reaction mixture and, consequently, any conclusions are necessarily tentative.

References

1. For a recent review, see C. Fedorchuk, M. C. Copsey, and T. Chivers. Coord. Chem. Rev. **251**, 897 (2007).
2. For recent papers on transition-metal complexes, see (a) D. R. Manke and D. G. Nocera. Inorg. Chem. **42**, 4431 (2003); (b) D. R. Manke, Z-H. Loh, and D. G. Nocera. Inorg. Chem. *43*, 3618 (2004).
3. T. Chivers, C. Fedorchuk, G. Schatte, and M. Parvez. Inorg. Chem. **42,** 2084 (2003).
4. T. Chivers, D. J. Eisler, C. Fedorchuk, G. Schatte, H. M. Tuononen, and R. T. Boeré. Chem. Commun. 3930 (2005).

5. T. Chivers, D. J. Eisler, C. Fedorchuk, G. Schatte, and H. M. Tuononen. Inorg. Chem. **45**, 2119 (2006)

6. D. R. Manke and D. G. Nocera. Polyhedron, **25**, 493 (2006).

7. D. Fest, C. D. Habben, A. Meller, G. M. Sheldrick, D. Stalke, and F. Pauer. Chem. Ber. **123**, 703 (1990).

8. T. Albrecht, G. Elter, M. Noltemeyer, and A. Meller. Z Anorg. Allg. Chem. **624**, 1514 (1998).

9. P. Paetzold, D. Hahnfeld, U. Englert, W. Wojnowski, B. Dreczewski, Z. Pawelec, and L. Walz. Chem. Ber. **125**, 1073 (1992).

10. W. Luthin, J.–G. Stratmann, G. Elter, A. Meller, A Heine, and H. Gornitzka. Z. Anorg. Allg. Chem. **621**, 1995 (1995).

11. A. Heine, D. Fest, D. Stalke, C. D. Habben, A. Meller, and G. M. Sheldrick. J. Chem. Soc., Chem. Commun. 742 (1990).

12. J. Konu, M. S. Balakrishna, T. Chivers, and T. W. Swaddle. Inorg. Chem. **46**, 2627 (2007).

13. T. Chivers, C. Fedorchuk, G. Schatte, and J. K. Brask. Can. J. Chem. **80**, 821 (2002).

14. (a) *WINEPR SimFonia*, version 1.25; Bruker Analytische; Messtechnik, Germany, 1996; (b) D. R. Duling *J. Mag. Res., Ser. B* **104**, 105 (1994).

15. G. M. Sheldrick. SHELXS-97, *Program for Crystal Structure Determination*, University of Göttingen, Germany, 1997.

16. G. M. Sheldrick. SHELXL-97, *Program for Crystal Structure Refinement*, University of Göttingen, Germany, 1997.

17. *Gaussian 03*, Revision C.02, M. J. Frisch, G. W. Trucks, H. B. Schlegel, G. E. Scuseria, M. A. Robb, J. R. Cheeseman, J. A. Montgomery, Jr., T. Vreven, K. N. Kudin, J. C. Burant, J. M. Millam, S. S. Iyengar, J. Tomasi, V. Barone, B. Mennucci, M. Cossi, G. Scalmani, N. Rega, G. A. Petersson, H. Nakatsuji, M. Hada, M. Ehara, K. Toyota, R. Fukuda, J.

Hasegawa, M. Ishida, T. Nakajima, Y. Honda, O. Kitao, H. Nakai, M. Klene, X. Li, J. E. Knox, H. P. Hratchian, J. B. Cross, V. Bakken, C. Adamo, J. Jaramillo, R. Gomperts, R. E. Stratmann, O. Yazyev, A. J. Austin, R. Cammi, C. Pomelli, J. W. Ochterski, P. Y. Ayala, K. Morokuma, G. A. Voth, P. Salvador, J. J. Dannenberg, V. G. Zakrzewski, S. Dapprich, A. D. Daniels, M. C. Strain, O. Farkas, D. K. Malick, A. D. Rabuck, K. Raghavachari, J. B. Foresman, J. V. Ortiz, Q. Cui, A. G. Baboul, S. Clifford, J. Cioslowski, B. B. Stefanov, G. Liu, A. Liashenko, P. Piskorz, I. Komaromi, R. L. Martin, D. J. Fox, T. Keith, M. A. Al-Laham, C. Y. Peng, A. Nanayakkara, M. Challacombe, P. M. W. Gill, B. Johnson, W. Chen, M. W. Wong, C. Gonzalez, and J. A. Pople, Gaussian, Inc., Wallingford CT, 2004.

18. (a) J. P. Perdew, K. Burke and M. Ernzerhof Phys. Rev. Lett. **77**, 3865 (1996); (b) J. P. Perdew, K. Burke and M. Ernzerhof Phys. Rev. Lett. **78**, 1396 (1997); (c) J. P. Perdew, K. Burke and M. Ernzerhof J. Chem. Phys. **105**, 9982 (1996); (d) M. Ernzerhof and G. E. Scuseria J. Chem. Phys. **110**, 5029 (1999).

19. (a) A. Schäfer, C. Huber and R. Ahlrichs J. Chem. Phys. **100**, 5829, (1994); (b) K. Eichkorn, F. Weigend, O. Treutler and R. Ahlrichs Theor. Chem. Acc. **97**, 119 (1197).

20. D. Andrae, U. Haeussermann, M. Dolg, H. Stoll and H. Preuss Theor. Chim. Acta **77**, 123 (1990).

21. (a) L. J. Laaksonen Mol. Graph. **33**, 10 (1992); (b) D. L. Bergman, L. Laaksonen and A. Laaksonen J. Mol. Graph. Model. **15**, 301 (1997).

22. J. Konu, H. M. Tuononen, T. Chivers, A. M. Corrente, R. T. Boeré, and T. Roemmele. Inorg. Chem. **47**, 3823 (2008).

23. (a) L. Pauling. "*The Nature of the Chemical Bond*", 3rd Ed., Cornell University Press, Ithaca, N.Y., 1960; (b) C. E. Housecroft and A. G. Sharpe. "*Inorganic Chemistry*", 2nd Ed., Pearson Education Ltd., Harlow,U.K., 2005.

24. M. Geschwentner, M. Noltemeyer, G. Elter, and A. Meller, Z Anorg. Allg. Chem. **620**, 1403 (1994).

25. H. Fusstetter, and H. Nöth. Chem. Ber. **112**, 3672 (1979).

26. S.-J.Kim, Y.-J. Lee, S. H. Kim, J. Ko, S. Cho, and S. O. Kang, Organometallics, **21**, 5358 (2002).

27. J. K. Brask and T. Chivers, Angew. Chem., Int. Ed. Engl. **40**, 3960 (2001).

Table 1. Crystallographic data for **1a**, **1b**, **2b,** and **2c**·THF.[a]

	1a	**1b**	**2b**	**2c**·THF
empirical formula	$C_{28}H_{46}B_2N_4Ge$	$C_{28}H_{46}B_2N_4Sn$	$C_{28}H_{46}B_2Li_2N_4Sn$	$C_{32}H_{54}B_2Li_2N_4OPb$
fw	532.90	579.00	592.88	753.48
cryst. system	orthorhombic	monoclinic	monoclinic	triclinic
space group	Pbcn	C2/c	$P2_1/c$	P-1
a, Å	17.259(4)	24.846(5)	13.544(3)	9.188(2)
b, Å	8.917(2)	8.738(2)	11.828(2)	10.201(2)
c, Å	20.256(4)	18.065(4)	20.059(4)	20.649(4)
α, deg.	90.00	90.00	90.00	79.05(3)
β, deg.	90.00	128.29(3)	104.72(3)	84.95(4)
γ, deg.	90.00	90.00	90.00	71.49(3)
V, $Å^3$	3117(1)	3078(2)	3108(1)	1801.1(7)
Z	4	4	4	2
T, ºC	-100	-100	-100	-100
ρ_{calcd}, g/cm^3	1.135	1.249	1.267	1.389
μ(Mo Kα), mm^{-1}	1.004	0.851	0.844	4.712
crystal size, mm^3	0.20x0.16x0.12	0.44x0.36x0.06	0.40x0.06x0.02	0.24x0.20x0.08
F(000)	1136	1208	1232	760
Θ range, deg	2.57-25.02	3.23-25.02	3.38-25.03	3.57-25.03
reflns collected	5083	5103	9846	12174
unique reflns	2732	2709	5430	6335
R_{int}	0.0213	0.0236	0.0457	0.0282
reflns [$I>2\sigma(I)$]	2066	2449	4020	5945
R_1 [$I>2\sigma(I)$] [b]	0.0360	0.0311	0.0468	0.0234
wR_2 (all data) [c]	0.0901	0.0808	0.0993	0.0555
GOF on F^2	1.059	1.033	1.103	1.032
completeness	0.990	0.996	0.991	0.996

[a] λ (MoKα) = 0.71073 Å. [b] $R_1 = \Sigma \big| |F_o| - |F_c| \big| / \Sigma |F_o|$. [c] $wR_2 = [\Sigma w(F_o^2-F_c^2)^2/\Sigma wF_o^4]^{½}$.

Table 2. Selected bond lengths (Å) and angles (°) in **1a** and **1b**

	1a[a]	**1b**[b]		**1a**[a]	**1b**[b]
M1-N1	1.846(2)	2.047(2)	B1-N1	1.438(3)	1.436(4)
M1-N2	1.842(2)	2.047(2)	B1-N2	1.439(4)	1.438(4)
N1-M1-N2	75.9(1)	69.2(1)	M1-N2-B1	90.2(2)	91.1(2)
N1-M1-N1’	128.6(1)[c]	129.2(2)[d]	N1-B1-N2	104.0(2)	107.9(2)
N1-M1-N2’	127.8(1)[c]	132.8(1)[d]	N1-B1-C9	127.3(2)	126.5(3)
N2’-M1-N2’	129.8(1)[c]	135.5(1)[d]	N2-B1-C9	128.7(2)	125.6(3)
M1-N1-B1	90.0(2)	91.2(2)			

[a] M = Ge, [b] M = Sn. Symmetry operation for the atoms marked with a single quote(‘); [c] -x, y, 0.5-z.; [d] 1-x, y, 1.5-z.

Table 3. Selected bond lengths (Å) and angles (°) in **2b** and **2c**·THF.

	2b[a]	**2c**·THF[b]		**2b**[a]	**2c**·THF[b]
M1-N1	2.194(4)	2.346(3)	Li2-N2	1.884(5)	1.974(6)
M1-N3	2.189(3)	2.335(3)	Li2-N4	2.557(6)	-
M1-N4	2.179(4)	2.309(2)	B1-N1	1.520(6)	1.490(4)
Li1-N2	1.915(9)	1.921(6)	B1-N2	1.408(7)	1.412(4)
Li1-N3	2.075(9)	2.039(6)	B2-N3	1.434(7)	1.447(5)
Li1-N4	2.115(9)	2.030(6)	B2-N4	1.466(6)	1.444(5)
Li2-N1	1.869(5)	2.055(6)			
N1-M1-N3	108.3(1)	99.5(1)	Li1-N3-B2	76.4(4)	77.7(2)
N1-M1-N4	99.1(1)	105.2(1)	M1-N3-Li1	84.7(3)	81.5(2)
N3-M1-N4	63.5(1)	59.8(1)	M1-N4-B2	89.7(3)	89.9(2)
N1-B1-N2	112.0(4)	112.9(3)	M1-N4-Li1	84.0(3)	82.3(2)
N3-B2-N4	104.9(4)	106.5(3)	Li1-N4-B2	74.5(3)	78.1(2)
M1-N1-B1	122.3(3)	120.1(2)	Li2-N4-B2	131.3(3)	-
Li2-N1-B1	80.5(3)	77.5(2)	N2-Li1-N3	132.7(5)	131.1(3)
M1-N1-Li2	89.5(2)	103.1(2)	N2-Li1-N4	121.9(4)	132.3(3)
Li1-N2-B1	108.2(4)	109.5(3)	N3-Li1-N4	66.5(3)	69.4(2)
Li2-N2-B1	82.8(3)	102.6(2)	N1-Li2-N2	80.6(2)	73.8(2)
Li1-N2-Li2	75.2(3)	88.7(3)	N4-Li2-N2	104.0(2)	-
M1-N3-B2	90.1(3)	88.8(2)			

[a] M = Sn, [b] M = Pb

Figure Captions

Fig. 1. Molecular structure of Ge[PhB(μ-N-*t*-Bu)$_2$]$_2$ (**1a**) with the atomic numbering scheme. Hydrogen atoms have been omitted for clarity. The tin complex **1b** is isostructural with **1a**. Symmetry operation: [a] -x, y, 0.5-z (M = Ge); 1-x, y, 1.5-z (M = Sn).

Fig. 2. (a) Simulated and (b) experimental EPR spectra of {Sn[PhB(μ-N-*t*-Bu)$_2$]$_2$}$^{\bullet+}$Cl$^-$ measured in diethyl ether at -20 ^{o}C.

Fig. 3. SOMO of the radical cation {Sn[PhB(μ-N^{t}Bu)$_2$]$_2$}$^{\bullet+}$ (±0.05 isodensity surfaces).

Fig. 4. Crystal structures of (a) Li$_2$Sn[PhB(μ-N-*t*-Bu)$_2$]$_2$ (**2b**) and (b) (THF·Li)LiPb[PhB(μ-N-*t*-Bu)$_2$]$_2$ (**2c**·THF) with the atomic numbering scheme. Hydrogen atoms have been omitted for clarity.

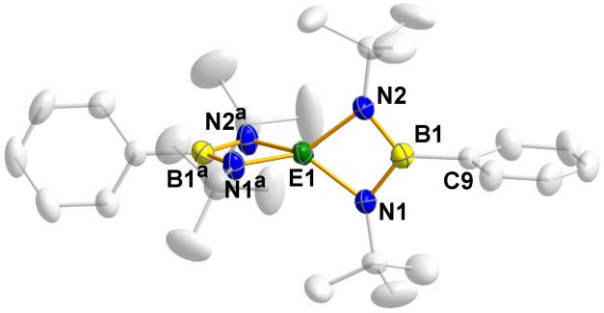

Fig. 1.

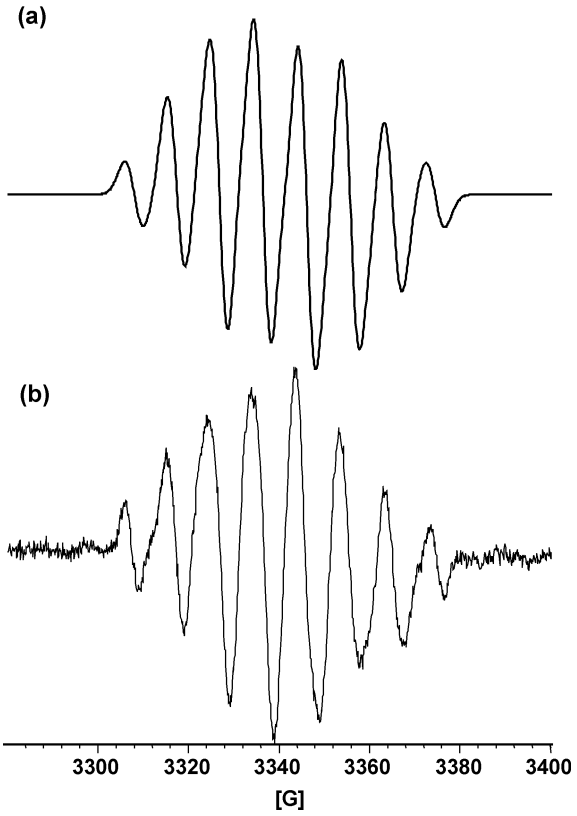

Fig. 2.

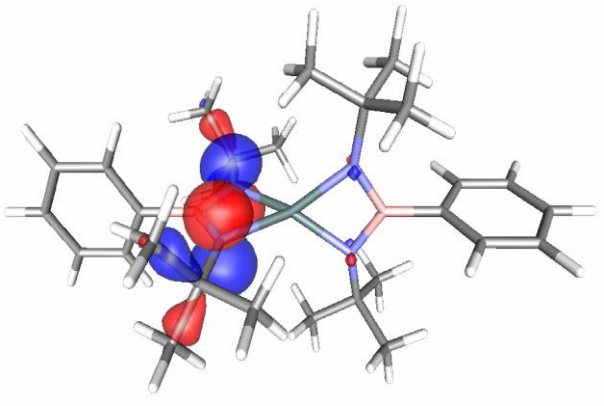

Fig. 3.

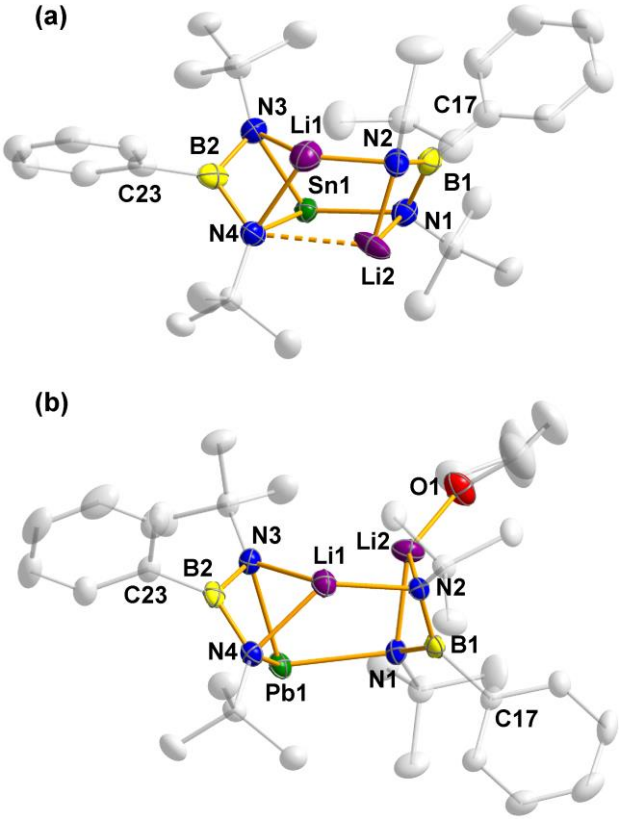
(a)
N3
Li1
C17
N2
B2
B1
C23
Sn1
N1
N4
Li2
(b)
O1
N3
Li2
Li1
B2
C23
N2
N4
B1
N1
Pb1
C17

Fig. 4.